Arch. Metall. Mater. **70** (2025), 2, 765-769

DOI: https://doi.org/10.24425/amm.2025.153478

J. LEE[1*], J. JEONG[1], J. JUNG[1,2], H. JEONG[1]

# OPTIMIZING DIELECTRIC CONSTANT IN TETRAGONAL $BaTiO_3$ VIA DENSIFICATION, TETRAGONALITY, AND GRAIN GROWTH KINETIC WITH SINTERING TEMPERATURE

Tetragonal $BaTiO_3$ nanopowders with tetragonality (c/a = 1.01), compacted uniaxially at 300 MPa, underwent sintering at temperatures ranging from 900°C to 1200°C for 1 h. Their densification and microstructure evolution were examined to determine the dielectric constant as a function of temperature (25-150°C) and frequency ($10^2$-$10^7$ Hz). Increasing the sintering temperature enhanced the densification and grain growth of $BaTiO_3$, demonstrating a linear relationship between them. However, the tetragonality remained unaffected by the sintering temperature. The densified $BaTiO_3$ exhibited a high dielectric constant ($\varepsilon_r$) across temperatures and frequencies. The activation energy for grain growth varied depending on the primary mechanism of lattice and grain boundary diffusion, ranging approximately from 119.1 to 172.5 kJ/mol across the entire sintering range.

*Keywords*: $BaTiO_3$; Sintering; Densification; Grain growth; dielectric constant

## 1. Introduction

Manufacturing ceramic products through conventional sintering processes is vital for their cost-effectiveness and the capability to yield materials with desirable properties. Densification of ceramic powder stands out as a critical factor in achieving these desired properties. Densification, which involves reducing porosity and increasing material density, holds significant importance as it profoundly impacts the mechanical, thermal, and electrical properties of the end product. Achieving optimal densification necessitates precise control over sintering conditions, including temperature, duration, and atmosphere, to facilitate appropriate particle bonding and grain growth [1].

Barium titanate (BTO), a widely studied ceramic material renowned for its outstanding dielectric properties, maintains stable capacity across a broad temperature range at high frequencies. The dielectric constant ($\varepsilon_r$) of BTO is known to correlate with factors such as tetragonality and powder size. Tetragonality, indicating the degree of distortion in the crystal lattice, directly influences polarization and, consequently, the material's dielectric behavior [2,3]. Similarly, $\varepsilon_r$ is significantly influenced by grain size in the ferroelectric state, whereas it remains nearly unaffected by grain size in the paraelectric state [4-7]. Previous research [1-7] has demonstrated that grain growth and densification during sintering have a significant impact on the dielectric permittivity. Despite these established relationships, there is a noticeable scarcity of studies exploring the interplay among densification, tetragonality, and dielectric constant in BTO at various sintering temperatures.

This study examines the correlations among dielectric constant, densification, tetragonality, and microstructural evolution in BTO ceramics sintered at various temperatures. Furthermore, grain growth kinetics are analyzed using Arrhenius modeling. The results of this investigation are expected to provide valuable insights into the optimization of sintering processes for tailoring the dielectric properties of BTO.

## 2. Experimental

The $BaTiO_3$ nanopowders, possessing a mean particle size of 217±5.6 nm, and a purity of 99.8% (KCM Corporation Co., Ltd., Japan), were prepared as illustrated in Fig. 1(a), which displays transmission electron microscopy (TEM) images along with a particle size distribution in the inserted plot. The nanopowders were compressed into cylindrical shapes with a diameter of 12.7 mm under a pressure of 300 MPa at room temperature. Subsequently, the samples underwent sintering at temperatures ranging from 900 to 1200°C for 1 h in an $N_2$ atmosphere to suppress grain growth caused by oxidation. The densities of

[1] KOREA INSTITUTE OF INDUSTRIAL TECHNOLOGY, MATERIALS SUPPLY CHAIN R&D DEPARTMENT, INCHEON CITY, 21999, REPUBLIC OF KOREA
[2] INHA UNIVERSITY, DEPARTMENT OF ADVANCED MATERIALS SCIENCE AND ENGINEERING, INCHEON CITY, 22212, REPUBLIC OF KOREA

* Corresponding author: ljb01@kitech.re.kr

samples sintered at different temperatures were determined using the Archimedes method. The crystal structures of the sintered samples were identified via X-ray diffraction (XRD) utilizing a Rigaku SmartLab instrument (Cu Kα, $\lambda$ = 1.54059 Å, 25 mA × 40 kV power), while their microstructure evolution was examined by scanning electron microscopy (SEM) at an accelerating voltage of 20 kV (SU5000, Hitachi, Tokyo, Japan). The dielectric constant ($\varepsilon_r$) was determined using a Novocontrol Concept 80 broadband dielectric spectrometer (Novocontrol Ltd, Germany), operating within the frequency range of $10^2$-$10^7$ Hz, and across temperatures from room temperature to 150°C. The mean grain size of the samples prepared under different conditions was statistically assessed based on recorded images and calculated using image analysis software (Image-Pro, Media Cybernetics Inc.). Mean grain size was determined by using the following Eq. (1) [8]

$$G = 1.56 \times L \quad (1)$$

where $G$ is the mean grain size, and $L$ is the mean grain boundary length for approximately 100 grains.

## 3. Results and discussion

Figs. 1(b) and 1(c) display SEM images of surface $BaTiO_3$ samples sintered at 900°C and 1100°C for 1 h, respectively. In these images, both the grain size and the length of the interconnected particles, known as neck growth, increased with annealing temperatures. Notably, in Fig. 1(c), the neck length is influenced by the size difference between interconnecting particles, which enlarges with increasing size disparity. While the particle size distribution in this study exhibited a unimodal pattern as seen in the Fig. 1(a), closer examination revealed a narrower distribution around 190-250 nm. Consistent with previous studies [9], as illustrated in Figs. 1(b) and (c), necking growth was more pronounced between particles of different sizes. Moreover, higher sintering temperatures promote increased mass transfer mechanisms responsible for grain growth by facilitating atomic movement along particle boundaries [10]. In Fig. 1(d), the mean grain size demonstrates a proportional relationship with the sintering temperature, suggesting that capillary stress, driven by surface energy, drives surface movement during sintering.

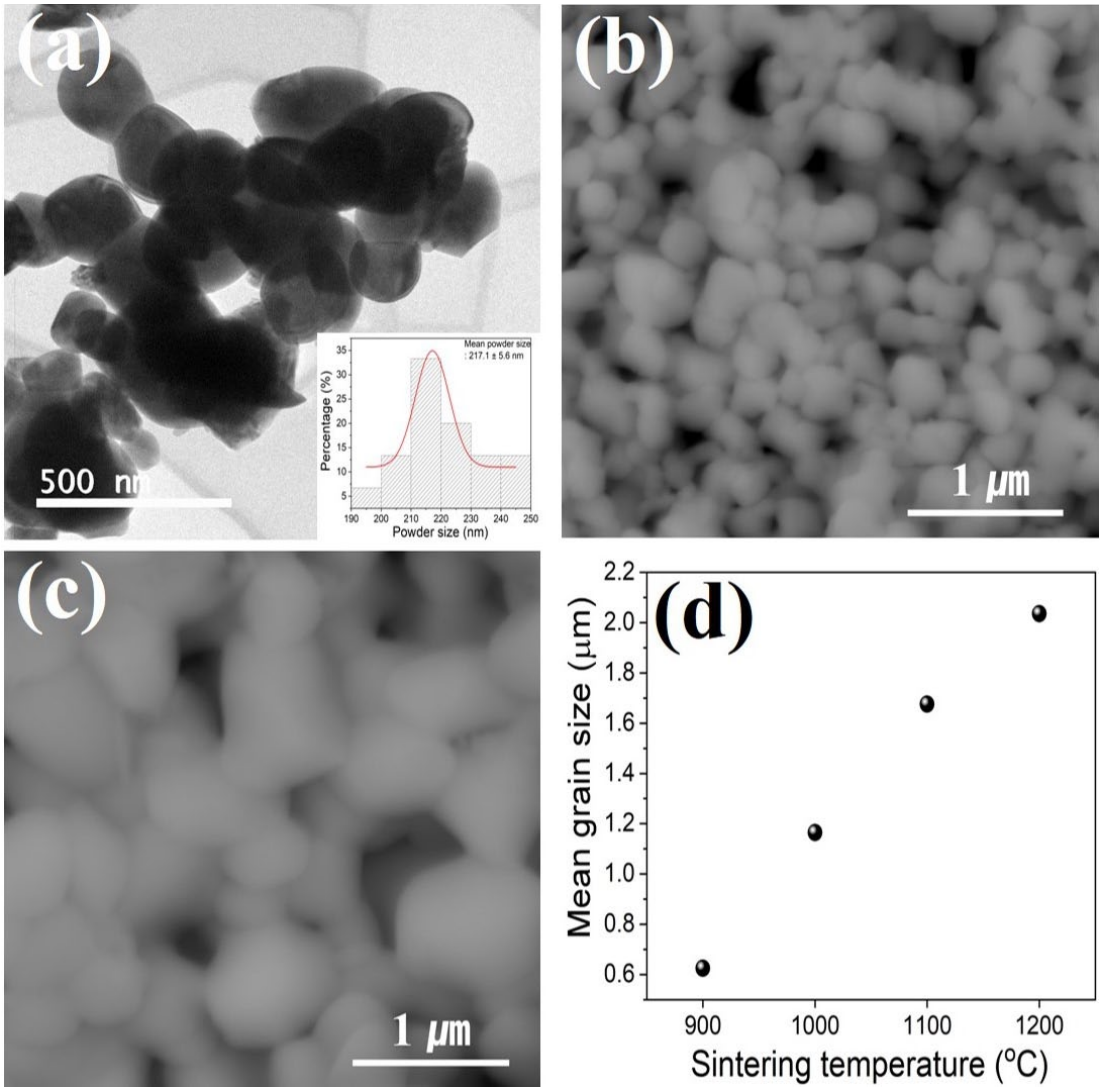


Fig. 1. (a) TEM image and particle size distribution (inserted plot) of as-received $BaTiO_3$ nanopowders, SEM images of the surface of samples sintered at (b) 900°C and (c) 1100°C for 1 h, and (d) plot of mean grain size for sintering temperatures

Notably, particle necks exhibit significant curvature changes. The Laplace equation provides the stress associated with a curved surface as follows:

$$\sigma = \gamma\left(\frac{1}{R_1}+\frac{1}{R_2}\right) \quad (2)$$

where $\gamma$ is the surface energy, and $R_1$ and $R_2$ are the radii of curvature for the surface. Spheres have uiform stress, but sintering alters their radii, causing non-uniform stress, as seen in saddle surfaces. The microstructure comprises convex and concave surfaces, shifting from tension to compression over distances smaller than the particle size and removing gradients naturally, thereby resulting in grain growth [11].

Fig. 2(a) depicts the variation of the dielectric constant ($\varepsilon_r$) of $BaTiO_3$ samples sintered at different temperatures relative to temperature, at a measurement frequency of 100 Hz. The $\varepsilon_r$ value of $BaTiO_3$ samples increased with rising sintering temperature, attributed to the increase in grain size in Fig. 1. Additionally, the sintered samples exhibit a broad peak in $\varepsilon_r$ around 130°C, consistent with findings from previous studies [12-13], indicating a ferroelectric phase transition. Above 130°C, the $\varepsilon_r$ value decreases with increasing in temperature, in accordance with the Curie-Weiss law:

$$\frac{1}{\varepsilon_r} = \frac{T - T_{C-W}}{C} \quad (2)$$

where $C$ is the Curie-Weiss constant, $T$ is the absolute temperature and $T_{C-W}$ is the Curie-Weiss temperature, which represents the beginning of the deviation of the dielectric constant from the Curie-Weiss law. Fig. 2(b) illustrates the relationship between frequency and dielectric constant in the $BaTiO_3$ samples sintered at various temperatures. Within the frequency range of $10^2$-$10^7$ Hz, the $\varepsilon_r$ value increased for samples sintered at higher temperatures, while it gradually decreased with increasing frequency across all samples. At lower frequencies, the higher $\varepsilon_r$ value was attributed to the presence of electronic, ionic, dipolar, atomic, and interfacial charge polarizations. The decrease in $\varepsilon_r$ value at higher frequencies is attributed to the presence of space charge polarization, reflecting the contribution of polarons [14]. At low frequencies, all polarization mechanisms (electronic, ionic, dipolar, and interfacial) contribute to the overall dielectric constant. As the frequency increases, the contribution of slower polarization mechanisms, such as dipolar and interfacial polarization, diminishes. This results in a decrease in the dielectric constant. At very high frequencies, only the rapid electronic polarization remains active, leading to a relatively constant and lower dielectric constant.

To investigate the factors influencing the dielectric constant, we determined the tetragonality (c/a) using XRD patterns obtained through the powerful Rietveld refinement method software (Crystal Impact GbR, Germany), as displayed in Fig. 3(a), against sintering temperature. Generally, higher tetragonality leads to a higher dielectric constant for $BaTiO_3$ ceramics. Tetragonality in Perovskite materials is roughly proportional to the magnitude of spontaneous polarization (Ps), hence exhibiting a linear relationship with the dielectric constant [3]. The tetragonality was found to remain nearly constant at 1.009-1.01 in Fig. 3(a), even with increasing sintering temperature. Previous studies have reported an increase in tetragonality with rising temperature, attributed to the elimination of OH groups present during BTO synthesis [15]. The absence of OH groups in the BTO used in this study explains the lack of variation in tetragonality with sintering temperature. Despite nearly consistent tetragonality across different sintering temperatures, the $\varepsilon_r$ value exhibited a positive correlation with sintering temperature, as shown in Fig. 2(a). Therefore, in this study, tetragonality was found to be independent of sintering temperature and not attributable to an increase in $\varepsilon_r$ value. Fig. 3(b) illustrates the relationship between relative density and grain size during the sintering process. Grain size increased with rising sintering temperature, leading to an increase in relative density. Both parameters exhibit a linear relationship (Figs. 2(b) and 3(b)). Previous studies [2], have reported that an increase in grain size elevates the tetragonality.

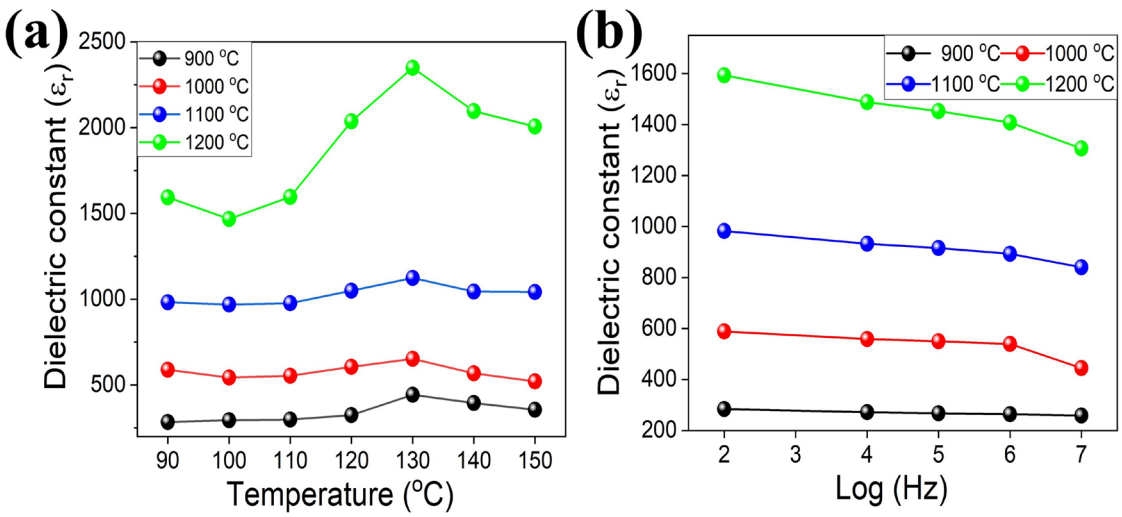


Fig. 2. Dielectric constant versus (a) temperature curve ranging from 90 to 150°C, and (b) frequency curve ranging from $10^2$ to $10^7$ Hz for the sintered samples

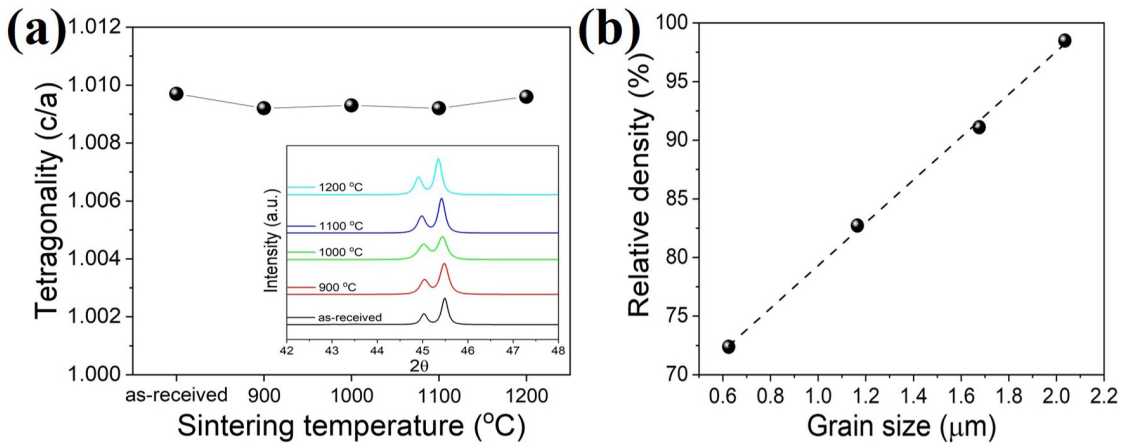


Fig. 3. (a) Variation in tetragonality (c/a) resulting from XRD patterns. (b) Relationship between relative density and grain size across all the samples

The grain growth kinetics can be expressed as [16]

$$G_t^n - G_0^n = Kt \tag{3}$$

where $G_t$ is the grain size at a given time, $G_0$ is the initial grain size, $n$ is the grain-growth exponent, $K$ is a constant, and $t$ is the sintering time. The variable $n$ represents the grain-growth behavior, and its value can be divided by the diffusion mechanism of pore control as follows: $n$ = 2 for grain boundary diffusion, and $n$ = 3 for vapor transport and lattice diffusion [17]. The activation energy ($Q$, kJ/mol) for grain growth within the sintered BTO samples at various temperatures was calculated based on the Arrhenius behavior [18].

$$K = K_0 \exp\left(-\frac{Q}{RT}\right) \tag{4}$$

where $K_0$ is a constant, $R$ is the gas constant (=8.314 J/(mol·K)), and $T$ is the absolute temperature. $Q$ is the log of both sides of Eq. (3) as follows:

$$\ln\left(G_t^n - G_0^n\right) = \ln K_0 + \ln t - Q/RT \tag{5}$$

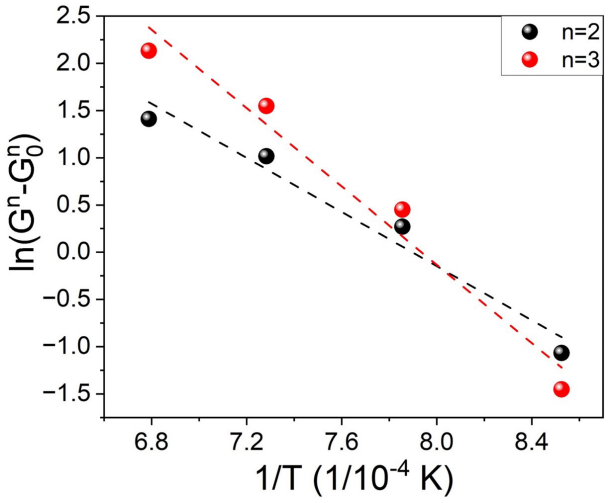


Fig. 4. Arrhenius plot of grain growth with at different sintering temperatures

Eq. (5) shows that ln$G$ and 1/$T$ exhibit a linear relationship at the same sintering time for both $n$ values 2 and 3, as illustraed in Fig. 4. The slope of this line indicates the activation energy for grain growth. Based on the graph results, it can be inferred that necking between the bonded powders occurs through vapor transport and lattice diffusion, while at higher temperatures, grain growth is facilitated by grain boundary diffusion. Over a wide temperature range, the BTO powders used required an activation energy of approximately 119.1 to 172.5 kJ/mol for grain growth.

## 4. Conclusion

This study investigated the densification and microstructure evolution of tetragonal $BaTiO_3$ nanopowders compacted uniaxially at 300 MPa and sintered at temperatures ranging from 900°C to 1200°C for 1 h. Increased sintering temperatures led to grain growth and densification, resulting in higher relative density and dielectric constant. This indicates that densification is crucial for achieving high dielectric properties. Interestingly, the tetragonality (c/a) remained unaffected by changes in temperature. The densified $BaTiO_3$ exhibited a high dielectric constant ($\varepsilon_r$) across a wide temperature range (25-150°C) and frequency range ($10^2$-$10^7$ Hz). Furthermore, the activation energy for grain growth, indicative of lattice and grain boundary diffusion mechanisms, ranged from approximately 119.1 to 172.5 kJ/mol throughout the entire sintering process.

### Acknowledgments

This study was supported by a materials & components technology development program funded by the Ministry of Trade, Industry, and Energy (MOTIE) (No. 20016519, Development of Ultra-Wide Band communication MLCC for UWB and 5G), and grant number 20022463.

## REFERENCE


[1] N. Shaw, Powder. Metall. Int. **25**, 25-29 (1989). https://www.osti.gov/etdeweb/biblio/5948159

[2] S. Yoon, M. Kim, D. Kim, J. Mater. Chem. C. **8**, 9373 (2020). DOI: https://doi.org/10.1039/D0TC02067B

[3] T. Qi, I. Grinberg, A. Rappe, Phys. Rev. B. **83**, 134113 (2010). DOI: https://doi.org/10.1103/PhysRevB.82.134113

[4] K. Kinoshita, A. Yamaji, J. Appl. Phys. **47**, 371-373 (1976). DOI: https://doi.org/10.1063/1.322330

[5] Y. Chen, H. Ye, X. Wang, Y. Li, X. Yao, J. Eur. Ceram. Soc. **40**, 391-400 (2020). DOI: https://doi.org/10.1016/j.jeurceramsoc.2019.09.0336

[6] M. Reavley, H. Guo, J. Yuan, A. Ng, T. Ho, H. Tan, Z. Du, C. Gan, J. Eur. Ceram. Soc. **42**, 4934-4943 (2022). DOI: https://doi.org/10.1016/j.jeurceramsoc.2022.04.056

[7] S. Paliwal, P. Mondal, A. Singh, Mater. Chem. Phys. **312**, 128613 (2024). DOI: https://doi.org/10.1016/j.matchemphys.2023.128613

[8] M. Mendelson, J. Am. Ceram. Soc. **52**, 443-446 (1969). DOI: https://doi.org/10.1111/j.1151-2916.1969.tb11975.x

[9] C. Chen, J. Yeom, C. Choe. et al., J. Mater. Sci. **54**, 13344-57 (2019). DOI: https://doi.org/10.1007/s10853-019-03813-0

[10] L. Singh, A. Bhadauria, S. Jana, T. Laha, Acta Metall. Sin. (Engl. Lett.) **31**, 1019-1030 (2018). DOI: https://doi.org/10.1007/s40195-018-0795-4

[11] Z.Z. Fang, Sintering of Advanced Materials: Fundamentals and Processes. Woodhead Publishing, Cambridge, UK, (2010). https://www.sciencedirect.com/book/9781845695620/sintering-of-advanced-materials#book-info

[12] S. Sharma, K. Shamim, A. Ranjan, R. Rai, P. Kumari, S. Sinha, Ceram. Int. **41**, 7713-7722 (2015). DOI: https://doi.org/10.1016/j.ceramint.2015.02.102

[13] A. Rached, M. Wederni, K. Khirouni, S. Alaya, R. Martín-Palma, J. Dhahri, Mater. Chem. Phys. **267**, 124600 (2021). DOI: https://doi.org/10.1016/j.matchemphys.2021.124600

[14] M. Sridhar Panday, M. Vinoth, S. Surendhiran, V. Rajendran, P. Susthitha Menon, IEEE International Conference on Semiconductor Electronics, ICSE, August, 192-196 (2016). DOI: https://doi.org/10.1109/smelec.2016.7573624

[15] J. Lee, H. Jeong, S. Ma, Mater. Res. Express. **9**, 065001 (2022). DOI: https://doi.org/10.1088/2053-1591/ac73e2

[16] F. Gil, J. Picas, J. Manero, A. Forn, J. Planell, J. Alloys Compd. **260**, 147-152 (1997). DOI: https://doi.org/10.1016/S0925-8388(97)00135-7

[17] F.F.Y. Wang, Ceramic Fabrication Processes: Treatise on Materials Science and Technology. Elsevier: London, UK, **9** (2016). https://shop.elsevier.com/books/ceramic-fabrication-processes/wang/978-0-12-341809-8

[18] B. Milsom, H. Porwal, G. Viola, Z. Gao, M. Reece, Mater. Des. **133**, 325-331 (2017). DOI: https://doi.org/10.1016/j.matdes.2017.07.040